Evidence for Interlayer Coupling and Moiré Periodic Potentials in Twisted Bilayer Graphene

Taisuke Ohta,[1] Jeremy T. Robinson,[2] Peter J. Feibelman,[1] Aaron Bostwick,[3] Eli Rotenberg,[3] and Thomas E. Beechem[1]

[1]*Sandia National Laboratories, Albuquerque, New Mexico 87185, USA*
[2]*Naval Research Laboratory, Washington, D.C. 20375, USA*
[3]*Advanced Light Source, Lawrence Berkeley National Laboratory, Berkeley, California 94720, USA*

We report a study of the valence band dispersion of twisted bilayer graphene using angle-resolved photoemission spectroscopy and *ab initio* calculations. We observe two noninteracting cones near the Dirac crossing energy and the emergence of van Hove singularities where the cones overlap for large twist angles ($> 5°$). Besides the expected interaction between the Dirac cones, minigaps appeared at the Brillouin zone boundaries of the moiré superlattice formed by the misorientation of the two graphene layers. We attribute the emergence of these minigaps to a periodic potential induced by the moiré. These anticrossing features point to coupling between the two graphene sheets, mediated by moiré periodic potentials.

Much effort has been directed toward using graphene in electronics and optoelectronics to exploit its high electrical conductivity and unique Dirac fermion quasiparticles [1]. With continuing progress in fabricating large-area graphene sheets, [2,3] one can now transfer one or a few graphene layers onto desired substrates [4] or construct hybrid multilayer structures [5,6]. Such transfer processes unavoidably introduce azimuthal misorientation, or twist. Many growth processes also result in twisted multilayers [7–9]. Envisioning applications involving more than one graphene sheet for specific properties [10–12] therefore makes it important to understand the electronic properties of "twisted graphene" [13].

A key issue is the electronic interaction between twisted graphene layers. Theoretical approaches have shown that, for twisted bilayer graphene (TBG), interlayer interaction occurs at discrete locations within the Brillouin zone (BZ) [14–18]. Depending on the twist angle, one can expect Fermi velocity reductions or the emergence of van Hove singularities (vHs). Transport measurements imply that TBG's charge carriers near the Dirac crossing energy (E_D) behave as if in an isolated graphene sheet, confirming theoretical predictions for a large twist angle [19,20]. Scanning tunneling microscopy and Raman spectroscopy support the notion of interlayer interaction through the presence of vHs [21–23] and a moiré [24]. On the contrary, angle-resolved photoemission spectroscopy (ARPES) investigations of a similar system, twisted *multilayer* graphene [i.e., >two layers, typically grown on the carbon face of silicon carbide (SiC)], provided no evidence of interlayer interaction across the entire BZ [25–27], despite formation of moiré [28]. So far, ARPES has provided little information regarding the TBG's interlayer interaction [29]. Thus, questions remain on the existence, extent, and origin of its interlayer interaction of the twisted graphene system.

We present a comprehensive picture of electronic dispersion in TBG, the simplest twisted graphene system, based on ARPES and density functional theory (DFT) calculations. We observed a band topology consisting of two noninteracting Dirac cones near E_D, and vHs and associated minigaps away from E_D, where the two layers' Dirac cones overlap. Our experimental results provide unambiguous evidence of the interlayer interaction in TBG. What is more, we observed additional minigaps at the boundaries of the superlattice BZ associated with the moiré that evolves as two graphene lattices are rotated with respect to one another. Our results show that a moiré superlattice gives rise to a periodic potential, altering the electronic dispersion across the entire BZ according to its long-range periodicity and not just where the states from two layers overlap. These observations illustrate how electronic dispersion is modulated by the moiré, a structure ubiquitous in superimposed two-dimensional (2D) lattices (e.g., hybrid multilayer structures [5,6]).

We fabricated TBG samples by transferring graphene monolayers grown on copper foils via chemical vapor deposition [2,3,30] onto single-crystalline epitaxial graphene monolayers grown on a hydrogen-terminated SiC (0001) (Si face) [31,32] following Ref. [33]. This fabrication procedure results in >100 μm domains with random rotational orientation between two graphene lattices. Within each domain, the twist angle is relatively constant [34]. Such samples allow a systematic ARPES study of electronic dispersion primarily on a single domain with minimal effect from the underlying substrate [35]. The underlayer's Dirac cone is fixed in momentum space (k space), while the overlayer's rotates about the Γ point of the first primitive BZ, depending on the twist angle θ [33]. ARPES measurements were conducted at beam line 7.0 of the Advanced Light Source [36] by using 95 eV photons, a spot size of $\sim 50 \times 100$ μm^2, and sample

1. REPORT DATE **02 NOV 2012**	2. REPORT TYPE	3. DATES COVERED **00-00-2012 to 00-00-2012**
4. TITLE AND SUBTITLE **Evidence for Interlayer Coupling and Moire Periodic Potentials in Twisted Bilayer Graphene**		5a. CONTRACT NUMBER
		5b. GRANT NUMBER
		5c. PROGRAM ELEMENT NUMBER
6. AUTHOR(S)		5d. PROJECT NUMBER
		5e. TASK NUMBER
		5f. WORK UNIT NUMBER
7. PERFORMING ORGANIZATION NAME(S) AND ADDRESS(ES) **Naval Research Laboratory,Electronic Science and Technology Division,Washington,DC,20375**		8. PERFORMING ORGANIZATION REPORT NUMBER
9. SPONSORING/MONITORING AGENCY NAME(S) AND ADDRESS(ES)		10. SPONSOR/MONITOR'S ACRONYM(S)
		11. SPONSOR/MONITOR'S REPORT NUMBER(S)

12. DISTRIBUTION/AVAILABILITY STATEMENT
Approved for public release; distribution unlimited

13. SUPPLEMENTARY NOTES

14. ABSTRACT

15. SUBJECT TERMS

16. SECURITY CLASSIFICATION OF:			17. LIMITATION OF ABSTRACT	18. NUMBER OF PAGES	19a. NAME OF RESPONSIBLE PERSON
a. REPORT **unclassified**	b. ABSTRACT **unclassified**	c. THIS PAGE **unclassified**	**Same as Report (SAR)**	**6**	

$T \sim 100$ K. Given the photon spot size, morphological variations at the micron scale [23] are averaged out in the ARPES measurement. Overall energy resolution was ~ 60 meV.

DFT calculations were conducted by using VASP [37] with the Ceperley-Alder local density functional [38], as parameterized by Perdew and Zunger [39], in the projector augmented wave approximation [40]. DFT inherently describes any interlayer electron hopping and interaction. We used a 400 eV plane-wave basis cutoff. Correspondingly, optimization of single-layer graphene yielded a C-C separation of 1.41 Å. Following Shallcross, Sharma, and Pankratov [15], we constructed a table of commensurate-moiré cell sizes, which revealed that a 11.64° twist angle corresponds to a TBG supercell with a repeat distance of 8.54 Å containing 292 carbon atoms (146 in each layer). This cell corresponds to Shallcross's parameters $p = 3$ and $q = 17$. The electronic band structure at this twist angle was computed for comparison to the ARPES data of nominally $\theta = \sim 11.6°$. We first obtained a self-consistent TBG charge density corresponding to a 9×9 equally spaced sample of the 2D superlattice BZ that included the zone center. We then computed energy levels using that density. With a bilayer separation of 3.4 Å, local density approximation forces on carbon atoms along the bilayer normal were < 0.02 eV/Å.

In the plots shown here, calculated DFT data are shifted to align E_D with the Fermi level (E_F), expanded by 13% in energy to account for many-body interactions [41], and adjusted for the average doping of the sample [42]. The doping level (50 meV) was estimated so that the DFT data best match the ARPES data along two high-symmetry directions [Figs. 2(d) and 2(e)]. Unequal carrier concentrations between two graphene sheets were not considered in the calculation.

The electronic states of TBG can be described by two primitive BZs having a twist angle between them. The case of $\theta = 11.64°$ is illustrated in Fig. 1(a). The red hexagon is the primitive BZ for the underlayer graphene; the blue one corresponds to the overlayer graphene. The two small half circles overlaid on Figs. 1(a) and 1(b) are the measured photoemission intensity from two Dirac cones of TBG with $\theta = \sim 11.6°$ [43]. These intensities are the constant energy contour at 0.4 eV below E_F, which intersects the overlayer and underlayer cones centered at the K and K_θ points, respectively [44]. Complete separation of the photoemission intensity evidences that there is no sign of interaction between the cones close to E_D.

The overlayer and underlayer cones exhibit slightly different spectra as seen in Fig. 1(c), which shows photoemission spectra along the line connecting K and K_θ points. Owing to photoelectron attenuation, the underlayer cone (left cone at the K point) displays slightly lower intensity. Moreover, although the overlayer and the underlayer graphene sheets are both p-doped, their carrier concentrations appear slightly different as evidenced by their dispersions near E_D. That is, the size of the overlayer Fermi surface (or the opening of the cone at E_F) is slightly smaller than the underlayer's with E_D at about $E_F +$ 0.15 eV and $E_F + 0.2$ eV for the over- and underlayer, respectively. This small shift in E_D is attributable to the smaller influence of the substrate on the overlayer, a result of screening. Correspondingly, epitaxial graphene on hydrogen-terminated SiC is slightly p-type [32,45].

Unlike near E_D, interactions between the two Dirac cones *are* observed at higher electron binding energy. Figures 2(a)–2(c) show photoemission intensity patterns at $E_F - 0.8, -1.0$, and -1.3 eV, where the contours of the cones deviate significantly from the expected circular-to-triangular band topology of monolayer graphene [46]. The superlattice BZ (black hexagon) and its high-symmetry points Γ_s, K_s, and K'_s are overlaid on these experimental curves to highlight the superlattice's influence on the interlayer interaction. [Note, throughout, that subscript "s"
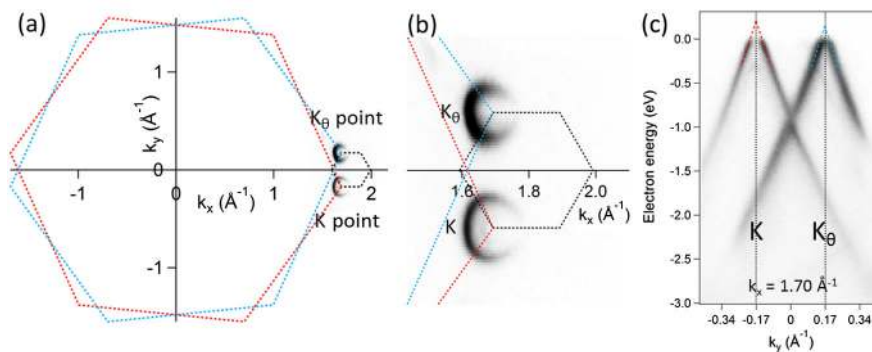

FIG. 1 (color online). k space representation of TBG with $\theta = \sim 11.6°$. (a) Photoemission intensity contour of the two Dirac cones at the electron energy $E_F - 0.4$ eV, and the primitive BZs of the underlayer and overlayer (red hexagon including the K point and blue one including the K_θ point). Darker shades indicate higher photoemission intensities. The small black hexagon is the moiré superlattice BZ of the $(p, q) = (3, 17)$ [15] commensurate TBG. (b) Enlarged image of (a) near the two cones. (c) Photoemission spectra intersecting two cones at K and K_θ points. The red (left) and blue (right) dashed lines illustrate the under- and overlayer cones, respectively, obtained by extrapolating the measured dispersions [62].
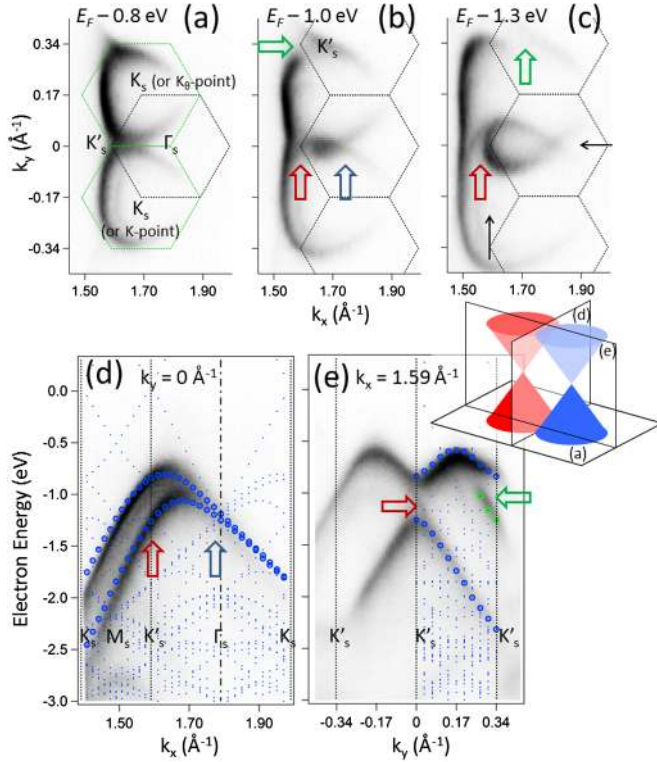
FIG. 2 (color online). Electronic dispersions of the two inter-acting Dirac cones ($\theta = \sim 11.6°$). (a)–(c) Photoemission inten-sity contours at $E_F - 0.8$ eV (a), $E_F - 1.0$ eV (b), and $E_F - 1.3$ eV (c). Black hexagons (thick line) indicate the moiré superlattice BZ of the commensurate TBG. Γ_s, K_s, and K'_s are among its high-symmetry points. K and K_θ points are both K_s points in the superlattice BZ. Green hexagons (thin line) are minizones of a continuum model with a Dirac point at its zone center. (d) Photoemission spectra and the DFT states bisecting the two cones and (e) the one orthogonal to (d). Their directions are indicated in (c) by horizontal and vertical black arrows. The schematic to the right of (e) shows the orientations of the photoemission patterns relative to the two primitive Dirac cones without interaction. DFT states are shown as (blue) dots. Calculated states matching the ARPES data are highlighted by blue (thick) and green (thin) circles.

indicates high-symmetry points associated with the *superlattice* BZ.] Note that while the cones exhibited "monolayerlike" topology near E_D [Figs. 1(a) and 2(a)], at higher binding energy, the two bands merge near the K'_s point [Fig. 2(b)]. This is a first indication of their interac-tion. At this intersection, nested parallel bands emerge to the left of the cones [i.e., towards the origin in k space as indicated by a red arrow in Figs. 2(b) and 2(c)], which exhibit an anticrossing behavior. This same behavior is not seen towards the right [cf. the blue arrow in Fig. 2(b)]. The reason is addressed below.

Emergence of the anticrossing of the two bands, or *minigap* formation, results from coupling between the two Dirac cones. To illustrate, Fig. 2(d) displays the pho-toemission spectra along the horizontal black arrow in Fig. 2(c), which bisects the two cones. Note that the π

state is split around the K'_s point (cf. the red arrow). This splitting is also seen in the DFT electronic levels [blue dots in Fig. 2(d)]. The anticrossing behavior can be understood in terms of vHs, when the orthogonal direction [vertical black arrow in Fig. 2(c)] is examined. Figure 2(e) shows photoemission spectra and DFT results along this direc-tion, where the upper "M"-shape and the lower inverted "V"-shape bands correspond to the left and right nested parallel bands in Fig. 2(c), respectively. By noting that the M-shaped band in Fig. 2(e) is the same as the upper split state in Fig. 2(d), it is apparent that these states have both positive and negative masses, creating a saddle point. Thus, as a consequence of coupling between the two layers' cones, vHs occur at the anticrossing.

Besides the vHs, faint states reside within the minigap near the red arrows in Figs. 2(c) and 2(e); however, they do not appear in the DFT calculation. We postulate that they are due to the areas where the interaction between two layers is reduced within a TBG domain. Such locations are attributable to topographical defects like ripples and blisters [47]. Low energy electron and atomic force micro-graphs support their presence on a length scale much smaller than our photon spot.

The photoemission intensity contours shown in Fig. 2 include an additional interacting feature not explained by direct interaction of the two layers' Dirac cones. The green arrows in Figs. 2(b) and 2(c) highlight a splitting in the overlayer cone around the K'_s point, along a direction extending into the upper-left superlattice BZ. For more details, we take a second derivative of the photoemission intensity with respect to electron energy, as shown in Fig. 3. Red and blue circles in Fig. 3(a) highlight under- and overlayer cones and help illustrate that the new feature appears not as a consequence of these cones' intersection but because of the presence of a "new" cone centered on the moiré superlattice K'_s point (black circle). Its disper-sion is displayed in Fig. 3(b), along a line from this new (black) cone to the overlayer (blue) cone [i.e., the green arrow in Fig. 3(a)]. Similar to the vHs observed in Fig. 2(e), an additional vHs is observed in both the ARPES and DFT results in Fig. 3(b). We attribute this new cone and the additional vHs forming along with it to adiabatic umklapp scattering in the superlattice periodic potential [48,49]. They could not be present if the electrons of one layer were not responding to the periodic potential imposed by the other, thus confirming that the two graphene layers are not isolated but sense each other.

The ramifications of the periodic potential applied to graphene (in this case induced by a moiré superlattice) should have intriguing consequences [50–52]. In "normal" 2D materials, applying a periodic potential results in the isotropic opening of the minigap over the entire boundary of the minizone defined by the potential's periodicity. Graphene's response is quite different because of the chiral (pseudospin) nature of the wave functions.
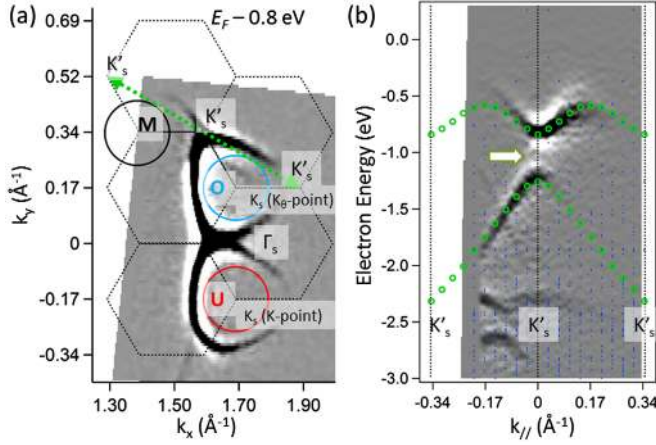
FIG. 3 (color online). Second derivative of the ARPES intensity with respect to the energy ($\theta = \sim 11.6°$). (a) Contours at $E_F - 0.8$ eV. The black hexagons are the superlattice BZ. The red, blue, and black circles with "U", "O," and "M" illustrate the locations of underlayer, overlayer, and moiré superlattice Dirac cones, respectively. (b) Processed photoemission pattern along the green arrow in (a) and DFT states (blue dots) connecting K'_s-K'_s-K'_s points. Circles (green) highlight DFT states matching the ARPES data.

Accordingly, the periodic potential does not open the minigap along the entirety of the minizone boundary but only at certain locations. Thus, moving along the minizone boundary, gaps will emerge and disappear.

To examine this effect, following Park *et al.* [51], we define the minizone [green hexagons in Fig. 2(a)] by translating the superlattice BZ, so the center of the superlattice BZ matches K and K_θ points. The line connecting K'_s and Γ_s points is along the minizone boundary [53]. In this view, coexistence of band splitting and crossing [shown by ARPES and DFT, red and blue arrows in Fig. 2(d)] is a consequence of the periodic potential induced by the moiré superlattice. Hence, the nonconstant gap occurs because of graphene's chiral wave functions.

Supporting this conclusion, the periodic potentials of a moiré should vary on a much longer length scale than the interatomic distance. Thus, a slight shift of one graphene sheet relative to another should only affect the electronic dispersion of TBG weakly. DFT calculations involving translations of one of the two graphene sheets by a fraction of interatomic distance confirm this. We conclude that TBG's electronic dispersion evolves from two rotated graphene sheets subject to a long-range potential of the moiré superlattice evolving between them. Alternatively, TBG comprises two graphene sheets, each subject to a periodic potential. This provides a simple way to understand many of the unique features alluded to in previous theoretical studies [51,52].

Incidentally, the additional interacting state does not appear at the underlayer cone highlighted by the red circle in the data presented but did appear in other data for different (typically smaller) twist angles [54]. If there is
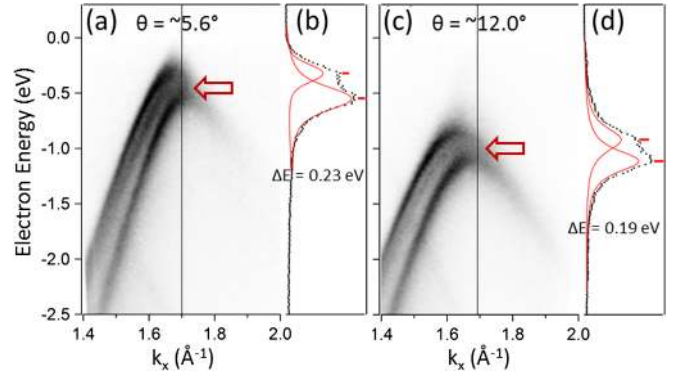

FIG. 4 (color online). Photoemission intensity patterns (a),(c) and EDCs (b),(d) displaying the minigap as a function of θ. (a), (b) $\theta = \sim 5.6°$, (c),(d) $\theta = \sim 12.0°$. The photoemission pattern bisects the two cones similarly to Fig. 2(d). (b) and (d) are EDCs at the black lines in (a) and (c), respectively, fitted to Voigt functions [thin (red) lines].

yet another new Dirac cone present in Fig. 3(a), we expect it to be centered on $k_x \sim 1.4$ Å^{-1}, $k_y \sim -0.34$ Å^{-1} and have the band topology similar to the new cone highlighted by the black circle. Although there is a state near where we expect to see the new cone, its shape is quite different. We therefore suspect that the data at the lower k_y in Fig. 3(a) originate from another TBG domain having a slightly different twist angle.

Regions of AB stacking in the moiré superlattice dominate the interlayer interaction for twist angles >5° [18], resulting in the minigaps seen in Fig. 4. Figures 4(b) and 4(d) show the energy distribution curves (EDCs) halfway between the K and K_θ points. For twist angles of ~5° to ~12°, the energy separation (peak-to-peak) stays near ~0.2 eV (cf. the red arrows). This value is of the same order of magnitude as the interlayer interaction parameter of Bernal bilayer graphene, ~0.4 eV [55]. We attribute the relatively unvarying magnitude of the minigap with twist angle to the persistence of local AB stacking within the moiré [56]. The large real-space moiré superlattice ensures the existence of AB stacking for all twist angles.

Last, we offer plausible rationales for the absence of some of our DFT energy levels in the corresponding ARPES data [see small blue dots in Figs. 2(d), 2(e), and 3(b)]. First, the structure factor associated with ARPES may preferentially increase the intensity of certain states. This has been observed in measurements wherein intensities are strongly enhanced when a surface state overlaps a bulk state in k space [57]. Following this argument, we presume that the TBG states overlapping those of a noninteracting graphene sheet would appear strongly in the ARPES measurement. Consequently, the measured photoemission intensity matches only a small subset of the DFT calculated states. Disorder in the TBG including mechanical distortions provides another possibility. As we saw via low energy electron diffraction, the twist angle in our samples varied

slightly, over a few micrometer length scale [33,34,58]. Because of the small superlattice BZ, the experimentally observed states from slightly different twist angles would be broadened with their intensity decaying rapidly, especially for those created by folding at superlattice BZ boundaries. The likelihood of observing these folded states would decrease correspondingly.

Coupling between the electronic states and the superlattice periodic potential have important implications for twisted multilayer graphene and hybrid 2D multilayer stacks. Based on our study of TBG, the superlattice BZ of a multilayer graphene ($>$ three layers) is expected to be smaller (thus longer periodicity in real space). Previous theoretical work has shown that, with an increase in spatial period, the apparent minigap shrinks [51], leading to effectively noninteracting states. This is consistent with reported experimental results [27]. Second, any hybrid multilayers based on transferring 2D materials will unavoidably induce moiré superlattices and thus subject the system to a periodic potential. This potential influences the dispersion and thus the properties of the multilayer stack. Although transfer techniques now offer the possibility of a wider class of 2D materials [59,60] much as heteroepitaxial growth does [61], understanding how these layers change as they are stacked together and mutually interact is prerequisite to leveraging their properties.

[1] A. H. Castro Neto, N. M. R. Peres, K. S. Novoselov, and A. K. Geim, Rev. Mod. Phys. **81**, 109 (2009).

[2] X. Li *et al.*, Science **324**, 1312 (2009).

[3] X. Li, C. W. Magnuson, A. Venugopal, R. M. Tromp, J. B. Hannon, E. M. Vogel, L. Colombo, and R. S. Ruoff, J. Am. Chem. Soc. **133**, 2816 (2011).

[4] M. Yankowitz, J. Xue, D. Cormode, J. D. Sanchez-Yamagishi, K. Watanabe, T. Taniguchi, P. Jarillo-Herrero, P. Jacquod, and B. J. LeRoy, Nat. Phys. **8**, 382 (2012).

[5] L. Britnell *et al.*, Science **335**, 947 (2012).

[6] H. Yan, X. Li, B. Chandra, G. Tulevski, Y. Wu, M. Freitag, W. Zhu, P. Avouris, and F. Xia, Nature Nanotech. **7**, 330 (2012).

[7] A. Reina, X. Jia, J. Ho, D. Nezich, H. Son, V. Bulovic, M. S. Dresselhaus, and J. Kong, Nano Lett. **9**, 30 (2009).

[8] J. Hass, F. Varchon, J. Millán-Otoya, M. Sprinkle, N. Sharma, W. de Heer, C. Berger, P. First, L. Magaud, and E. Conrad, Phys. Rev. Lett. **100**, 125504 (2008).

[9] S. Nie *et al.* (to be published).

[10] K. Kim, Y. Zhao, H. Jang, S. Y. Lee, J. M. Kim, K. S. Kim, J.-H. Ahn, P. Kim, J.-Y. Choi, and B. H. Hong, Nature (London) **457**, 706 (2009).

[11] S. Pang, Y. Hernandez, X. Feng, and K. Müllen, Adv. Mater. **23**, 2779 (2011).

[12] S. Ghosh, W. Bao, D. L. Nika, S. Subrina, E. P. Pokatilov, C. N. Lau, and A. A. Balandin, Nature Mater. **9**, 555 (2010).

[13] A. H. MacDonald and R. Bistritzer, Nature (London) **474**, 453 (2011).

[14] J. M. B. Lopes dos Santos, N. M. R. Peres, and A. H. Castro Neto, Phys. Rev. Lett. **99**, 256802 (2007).

[15] S. Shallcross, S. Sharma, and O. A. Pankratov, Phys. Rev. Lett. **101**, 056803 (2008).

[16] G. Trambly De Laissardière, D. Mayou, and L. Magaud, Nano Lett. **10**, 804 (2010).

[17] E. J. Mele, Phys. Rev. B **84**, 235439 (2011).

[18] R. Bistritzer and A. H. MacDonald, Proc. Natl. Acad. Sci. U.S.A. **108**, 12 233 (2011).

[19] H. Schmidt, T. Ludtke, P. Barthold, E. McCann, V. I. Fal'ko, and R. J. Haug, Appl. Phys. Lett. **93**, 172108 (2008).

[20] J. D. Sanchez-Yamagishi, T. Taychatanapat, K. Watanabe, T. Taniguchi, A. Yacoby, and P. Jarillo-Herrero, Phys. Rev. Lett. **108**, 076601 (2012).

[21] G. Li, A. Luican, J. M. B. Lopes dos Santos, A. H. Castro Neto, A. Reina, J. Kong, and E. Y. Andrei, Nat. Phys. **6**, 109 (2009).

[22] A. Luican, G. Li, A. Reina, J. Kong, R. Nair, K. Novoselov, A. Geim, and E. Andrei, Phys. Rev. Lett. **106**, 126802 (2011).

[23] K. Kim, S. Coh, L. Tan, W. Regan, J. Yuk, E. Chatterjee, M. Crommie, M. Cohen, S. Louie, and A. Zettl, Phys. Rev. Lett. **108**, 246103 (2012).

[24] A. Righi, S. Costa, H. Chacham, C. Fantini, P. Venezuela, C. Magnuson, L. Colombo, W. Bacsa, R. Ruoff, and M. Pimenta, Phys. Rev. B **84**, 241409(R) (2011).

[25] M. Sprinkle *et al.*, Phys. Rev. Lett. **103**, 226803 (2009).

[26] D. A. Siegel, C.-H. Park, C. Hwang, J. Deslippe, A. V. Fedorov, S. G. Louie, and A. Lanzara, Proc. Natl. Acad. Sci. U.S.A. **108**, 11 365 (2011).

[27] J. Hicks *et al.*, Phys. Rev. B **83**, 205403 (2011).

[28] D. L. Miller, K. D. Kubista, G. M. Rutter, M. Ruan, W. A. de Heer, M. Kindermann, P. N. First, and J. A. Stroscio, Nat. Phys. **6**, 811 (2010).

[29] C. Mathieu, N. Barrett, J. Rault, Y. Mi, B. Zhang, W. de Heer, C. Berger, E. Conrad, and O. Renault, Phys. Rev. B **83**, 235436 (2011).

[30] Graphene monolayers grown on copper foils via chemical vapor deposition typically consist of domains of a few hundred micrometers in size with random orientations.

[31] K. V. Emtsev *et al.*, Nature Mater. **8**, 203 (2009).

[32] C. Riedl, C. Coletti, T. Iwasaki, A. A. Zakharov, and U. Starke, Phys. Rev. Lett. **103**, 246804 (2009).

[33] T. Ohta, T. E. Beechem, J. Robinson, and G. L. Kellogg, Phys. Rev. B **85**, 075415 (2012).

[34] Using low energy electron microscopy and diffraction, we determined that the twist angle within each domain can vary up to 1° and typically has $\leq 0.5°$ variation over a few to tens of micrometers length scale.

[35] A. Bostwick, F. Speck, T. Seyller, K. Horn, M. Polini, R. Asgari, A. H. MacDonald, and E. Rotenberg, Science **328**, 999 (2010).

[36] Scienta R4000 electron energy analyzer.

[37] G. Kresse and J. Furthmüller, Comput. Mater. Sci. **6**, 15 (1996); Phys. Rev. B **54**, 11 169 (1996).

[38] D. M. Ceperley and B. J. Alder, Phys. Rev. Lett. **45**, 566 (1980).

[39] J. P. Perdew and A. Zunger, Phys. Rev. B **23**, 5048 (1981).

[40] P. E. Blöchl, Phys. Rev. B **50**, 17 953 (1994); G. Kresse and D. Joubert, Phys. Rev. B **59**, 1758 (1999).

[41] C. Heske, R. Treusch, F. Himpsel, S. Kakar, L. Terminello, H. Weyer, and E. Shirley, Phys. Rev. B **59**, 4680 (1999).

[42] T. Ohta, A. Bostwick, J. McChesney, T. Seyller, K. Horn, and E. Rotenberg, Phys. Rev. Lett. **98**, 206802 (2007).

[43] The twist angle is estimated from the ARPES data. The measured photoemission intensity is suppressed on one side of the BZ due to interference effects between the two equivalent sublattices in graphene. E. L. Shirley, L. J. Terminello, A. Santoni, and F. J. Himpsel, Phys. Rev. B **51**, 13 614 (1995).

[44] The other cones located at the corners of primitive BZs (K, K', K_θ, and K'_θ points) are not shown due to the limited k space of the measurement.

[45] A. L. Walter *et al.*, Phys. Rev. B **84**, 085410 (2011).

[46] A. Bostwick, T. Ohta, T. Seyller, K. Horn, and E. Rotenberg, Nat. Phys. **3**, 36 (2006).

[47] N. Levy, S. A. Burke, K. L. Meaker, M. Panlasigui, A. Zettl, F. Guinea, A. H. Castro Neto, and M. F. Crommie, Science **329**, 544 (2010).

[48] A. Mugarza and J. E. Ortega, J. Phys. Condens. Matter **15**, S3281 (2003).

[49] D. C. Tsui, M. Sturge, A. Kamgar, and S. Allen, Phys. Rev. Lett. **40**, 1667 (1978).

[50] N. Shima and H. Aoki, Phys. Rev. Lett. **71**, 4389 (1993).

[51] C.-H. Park, L. Yang, Y.-W. Son, M. L. Cohen, and S. G. Louie, Nat. Phys. **4**, 213 (2008).

[52] M. Barbier, F. M. Peeters, P. Vasilopoulos, and J. Milton Pereira, Jr., Phys. Rev. B **77**, 115446 (2008).

[53] To avoid confusion, we use the word ''minizone'' used for continuum models, which typically define the bottom of a parabolic state (equivalent to the Dirac crossing point) as the zone center. The superlattice BZ has the same reciprocal lattice vectors as the ones of the minizone, but the Dirac points are located at the corners.

[54] Given the precision of the sample goniometer we used for ARPES, we can typically acquire data from an area of the sample amounting to $\sim 50 \times 100$ μm^2 if the sample tilt is no more than $\sim 5°$. Near the Dirac point in our measurement, this tilt angle range corresponds to ~ 0.4 Å^{-1} in reciprocal space.

[55] T. Ohta, A. Bostwick, T. Seyller, K. Horn, and E. Rotenberg, Science **313**, 951 (2006).

[56] G. Trambly de Laissardière, D. Mayou, and L. Magaud, Phys. Rev. B **86**, 125413 (2012).

[57] Ph. Hofmann, Ch. Søndergaard, S. Agergaard, S. Hoffmann, J. Gayone, G. Zampieri, S. Lizzit, and A. Baraldi, Phys. Rev. B **66**, 245422 (2002).

[58] T. E. Beechem, B. Diaconescu, T. Ohta, and J. Robinson (unpublished).

[59] B. Radisavljevic, M. B. Whitwick, and A. Kis, ACS Nano **5**, 9934 (2011).

[60] D. Kim *et al.*, Nat. Phys. (to be published).

[61] T. Ando, A. B. Fowler, and F. Stern, Rev. Mod. Phys. **54**, 437 (1982), and references therein.

[62] A faint state around $E_F - 0.3$ eV in the left Dirac cone at the K point (underlayer) reflects a small coverage of the second layer in epitaxial graphene.